UCRL- 91506
PREPRINT
CONF - 8409157--5

PLASMA POTENTIAL FORMATION AND MEASUREMENT IN TMX-U AND MFTF-B

D. P. Grubb

This paper was prepared for presentation at the 5th Topical Conference on High Temperature Plasma Diagnostics, American Physical Society, Lake Tahoe, CA, Sept. 16-20, 1984.

September 28, 1984

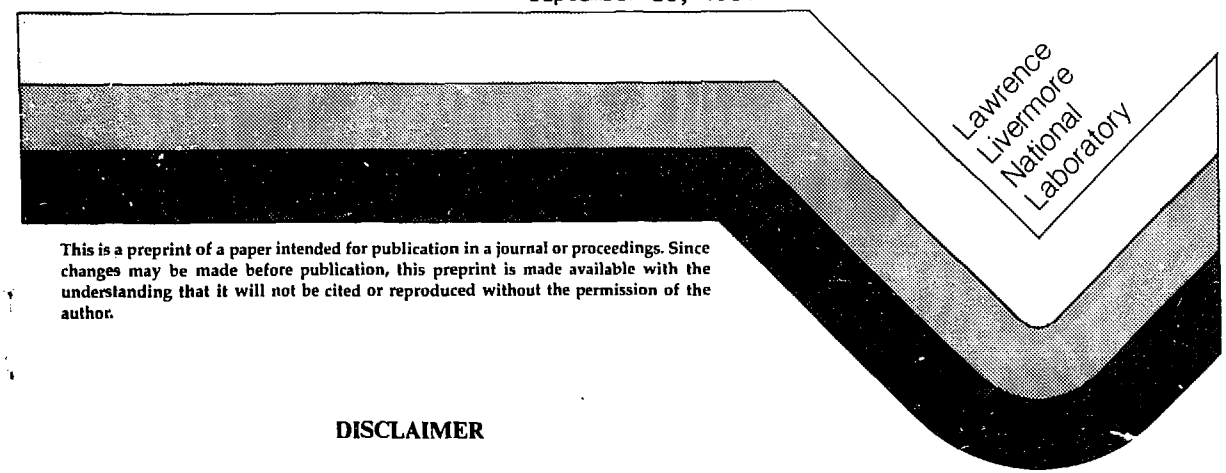

DISCLAIMER

UCRL--91506

DE85 002173

PLASMA POTENTIAL FORMATION AND MEASUREMENT IN TMX-U AND MFTF-B

D. P. Grubb
Lawrence Livermore National Laboratory, University of California
Livermore, CA 94550

ABSTRACT

Tandem mirrors control the axial variation of the plasma potential to create electrostatic "plugs" that improve the axial confinement of central cell ions and, in a thermal barrier tandem mirror, control the electron axial heat flow. Measurements of the spatial and temporal variations of the plasma potential are, therefore, important to the understanding of confinement in a tandem mirror. In this paper we discuss potential formation in a thermal barrier tandem mirror and examine the diagnostics and data obtained on the TMX-U device, including measurements of the thermal barrier potential profile using a diagnostic neutral beam and charged particle energy-spectroscopy. We then describe the heavy ion beam probe and other new plasma potential diagnostics that are under development for TMX-U and MFTF-B and examine problem areas where additional diagnostic development is desirable.

INTRODUCTION

In most mirror machines, the ions are less collisional than the electrons and are better confined by the mirrors. The plasma, therefore, charges up positively with respect to the walls of the confinement vessel as

the electrons escape to the ends of the device. The positive plasma potential increases, thereby reducing the electron flow until quasi-neutrality is satisfied where the ion and electron losses are equal. The resulting equilibrium plasma potential is given by the Pastukov relationship,[1]

$$\phi_e \approx T_e \ln \left[\frac{n\tau_i}{K\, T_e^{3/2}\, \phi_e/T_e} \right] , \qquad (1)$$

where T_e is the electron temperature, ϕ_e is the electron-confining potential, $n\tau_i$ is the product of the ion density by its confinement time, and K is equal to 5×10^8 for $\ln \Lambda = 15$, n in units of cm^{-3}, and ϕ and T in units of keV. [In Eq. (1) we have assumed a singly charged ion species and ignored the effects of secondary electron emission from the end walls.] The solution to Eq. (1) usually generates ϕ_e = 4 to 5 times T_e, as seen experimentally.

At low density ($n < 1 \times 10^{12}$ cm^{-3}) in the Tandem Mirror Experiment-Upgrade (TMX-U) at Lawrence Livermore National Laboratory (LLNL), we have observed values of ϕ_e/T_e as large as 20 to 30. This enhanced potential appears to be caused by electron-cyclotron resonance (ECR) trapping and scattering of electrons in the plugs, as predicted by Fokker-Planck and Monte-Carlo codes. At this time we do not have an analytic equation that accurately predicts these enhanced potentials.

It is this tendency for a mirror machine to charge up positively that led to the concept of a tandem mirror. In a standard tandem mirror, the end cell (plug) density is made higher than that of the central cell so that the plug potential is higher than that of the central cell by an amount $\phi_i = T_e \ln (n_p/n_c)$, where n_p and n_c are the plug and central cell densities, respectively. The positive potential difference ϕ_i between the central cell

potential ϕ_e and the plug potential ϕ_p electrostatically stops (plugs) the axial loss of all central cell ions with energies less than ϕ_i. The standard tandem mirror concept has been shown to work in several experiments.[2-4]

The standard tandem mirror requires $n_p > n_c$. This restriction leads to reactor designs with high density and temperature plugs that require very strong plug magnets and very energetic plug neutral-beam injectors. A thermal barrier[5,6] significantly reduces these reactor design problems by allowing the plug density to be lower than the central cell while maintaining a large electrostatic plugging potential for the central cell ions. A thermal barrier is a depression in the axial profile of the plasma potential, which isolates the central cell electrons from the electrons in the ion-confining potential peak. This isolation makes it possible to selectively heat the electrons at the potential peak.[7,8]

To understand how a thermal barrier works in a TMX-U end cell (Fig. 1), we must examine the relationship between the particle species that form the barrier: (a) sloshing ions, (b) hot electrons, and (c) potentially confined, warm electrons. The sloshing ions are created by injecting neutral beams at 47^o to the magnetic axis at the midplane of the plug. Because of the angle of injection, these energetic (10 keV) ions have turning points away from the midplane of the plug at a mirror ratio of approximately 2. As long as pitch-angle scattering and ion-to-electron energy exchange (drag) are slow processes on the time scale of the sloshing ion lifetime, the sloshing ions create axial density peaks near their turning points.

At the midplane of the end cell, hot mirror-confined electrons charge neutralize the sloshing ions. These energetic (20 to 200 keV) electrons are

first trapped by the fundamental electron-cyclotron resonant heating (ECRH) near the potential peak. They are subsequently heated by the fundamental until the second harmonic ECRH near the plug midplane becomes effective and increases their energy to the desired value. Because these electrons are energetic, they are almost as well mirror-confined as the sloshing ions. The plasma in this region maintains quasi-neutrality without charging up to a large positive potential. As a result, a potential dip develops between the central cell (where there are no hot, mirror-confined electrons) and the plug midplane (where the hot electron density peaks). This potential dip is the "thermal barrier" that isolates the central cell electrons from the electrons in the potential peak. The depth of the thermal barrier ϕ_b is given by

$$\phi_b = T_{ec} \ln [n_c/n_b (1 - f_{eH})] \quad , \tag{2}$$

where n_c and n_b are the total electron densities at the central cell and the plug midplane, respectively; f_{eH} is the ratio of the hot, mirror-confined electron density to the total density at the plug midplane; and T_{ec} is the central cell electron temperature. (Because the electron temperature along the field line is no longer constant, we differentiate the temperatures between the different species of electrons.)

The ion-confining potential peak forms at the outer sloshing-ion turning point. Here the hot electron density is not sufficient to charge neutralize the sloshing ions. This charge imbalance occurs because the sloshing-ion density peaks off the plug midplane. The hot electrons, however, are purposely formed so that their density peaks at the midplane. The difference between the sloshing ion density at the potential peak and the hot electron density is made up by warm, potentially confined electrons and a few energetic central cell electrons that can pass through the thermal barrier.

The fundamental ECRH at the potential peak increases the energy of the potentially confined, warm electrons so that they can escape the potential well that confines them. The plasma potential, however, must adjust to contain enough electrons at the potential peak to charge neutralize the sloshing ions. As the fundamental ECRH power is increased, therefore, the magnitude of the potential peak increases to maintain quasi-neutrality. This, correspondingly, increases the ion-confining potential and exponentially improves the central cell ion confinement.

The magnitude of the ion-confining potential depends upon the distribution function of the electrons in the potential peak. For Maxwellian electrons, ϕ_i is given by[7]

$$\phi_i = T_{ep} \ell n \left[(n_p/n_c)(T_{ec}/T_{ep})^{1/2}\right] - \phi_b \quad , \tag{3}$$

where T_{ep} is the temperature of the electrons in the potential peak and n_p is their density.

When the ECRH energy diffusion time is short compared to the electron scattering time, the electron distribution function is distorted. In the limit of very strong ECRH, the distribution function is constant along the heating characteristics, and the magnitude of the ion-confining potential (in TMX-U) becomes[8]

$$\phi_i = 2/3\ T_{ec} \left[n_p/n_b\ (1 - f_{eH})\right]^{2/3} \left[n_c/n_b\ (1 - f_{eH})\right]^{1/5} - \phi_b \quad . \tag{4}$$

This equation describes plugging in the strong ECRH regime and gives larger ϕ_i for a given plug to central cell density ratio than Eq. (3). The TMX-U machine appears to operate in this regime at densities less than 1×10^{12} cm^{-3} and

more like Eq. (3) at higher densities. Note that both Eqs. (3) and (4) produce positive values for ϕ_i even when $n_p < n_c$.

In this introductory section, we have examined the thermal barrier concept and determined the theoretical basis for thermal barrier formation. In the process we have shown that the critical potentials in a thermal barrier tandem mirror are ϕ_e, the central cell electron-confining potential; ϕ_b, the depth of the thermal barrier; ϕ_i, the ion confining potential; and ϕ_p, the maximum potential in the plug (the sum of $\phi_e + \phi_i$). In the next section we shall look at the TMX-U plasma potential diagnostics in use and those under development. In the last section we shall look ahead to diagnostic needs for the MFTF-B experiment.

I. PLASMA POTENTIAL DIAGNOSTICS FOR TMX-U

The TMX-U device was designed to demonstate thermal barrier formation in a tandem mirror. The typical magnetic field configuration produces end cells with a 4:1 axial mirror ratio (0.5 T at the plug midplane and 2 T at the outer mirror) and a 0.5% radial well depth for magnetohydrodynamic (MHD) stability. The field is mapped from the quadrupole field of the plugs through recircularizing coils into the solenoidal field of the central cell. In the process, the magnetic field is decreased from 2.2 T at the inner mirror of the plugs to 0.3 T at the central cell midplane.

There are a total of six neutral beams (15 kV, 50 A) on each TMX-U end cell to fuel the sloshing ions and to remove cold ions from the thermal barrier. An additional six neutral beams fire into the central cell to heat

and fuel the central cell at high density. To augment the heating at low density, we couple ion-cyclotron resonant heating (ICRH) power to the plasma using a pair of ICRH antennas--one at each of the central cell.

Two, pulsed, 28-GHz gyrotrons per end cell trap and heat the electrons. Each tube is capable of producing 200 kW of ECRH power. Using overmoded wave guides with polarizing reflectors, we launch 80 to 90% of the gyrotron power onto the plasma. The maximum pulse duration is 50 to 60 ms.

Because measurements of the plasma potential are important to understanding the confinement in a tandem mirror, the basic diagnostic set on TMX-U includes detectors capable of measuring both the spatial ar . te.mporal variations of the critical potentials ϕ_e, ϕ_b, ϕ_i, and ϕ_p. Fig. 2 shows the position of the TMX-U plasma potential diagnostics.

The first diagnostic, the end-loss analyzer (ELA), is a gridded, electrostatic particle-energy analyzer that is routinely used to measure the plug potential ϕ_p. Under special operating conditions (single end plug), it has been used to measure both the central cell potential ϕ_e and the depth of the thermal barrier ϕ_b. At this time there are five such analyzers on TMX-U: one on each end wall of the device, which is at a fixed radius of r $\simeq$ 0; one near each end wall of the device, which can be scanned radially across the thin dimension of the end fan; and one near the east end wall, which can be scanned radially across the long dimension of the end fan.

An ELA Fig. 3) consists of an entrance aperture and a series of grounded grids, followed by biased (repeller) grids, and finally a particle collector plate. The grounded grids reduce the particle flux entering the analyzer such that the grid spacing on the biased grids is larger than a Debye

length. They also insure that the bias on the repeller grids does not perturb the confined plasma. The first set of biased grids repels ions with energies less than the grid bias. The voltage on these grids is swept repeatedly in time to determine the energy spectrum of the end loss ions. The second set of biased grids is biased to repel incoming electrons and to reflect any secondary electrons that may be emitted from the collector surface. For a detailed report on the design of this analyzer see Ref. 9.

The time histories of the collected ion current and the applied ion repeller voltage during a TMX-U discharge are shown in Fig. 4. Also illustrated in this figure is the collected current versus the ion repeller voltage for one voltage sweep. The plateau in the I-V characteristic is caused by the escaping ions falling through a potential drop from the confined plasma region to the end wall where they pass through the grounded entrance grids of the ELA. When there is no ion-confining peak in the plug, the ELA measures the central cell potential ϕ_e (ELA2, Fig. 5). And when $\phi_i > 0$, the ELA measures the maximum potential in the plug (ELA3, Fig. 5).

This same diagnostic and analysis technique was modified to measure the depth of the thermal barrier potential dip ϕ_b in TMX-U. To make this measurement, we operated TMX-U as a single-end tandem mirror by injecting sloshing-ion neutral beams into the west plug but not the east. The expected axial potential profile during these experiments is shown in Fig. 5.

The maximum voltage that could be applied to the repeller grid of the ELA3 (2.4 kV) did not attenuate the already small ion current measured during plugging. This indicates that the plug plasma potential exceeded 2.4 kV. The difference between the plug potential and the measured central cell potential--the ion-confining potential--was, therefore, in excess of 1.4 kV.

ELA1 measured the axial potential variation in the thermal barrier region of the west plug by measuring the energy spread of the diagnostic neutral-beam-injected ions. A diagnostic neutral beam was injected into the thermal barrier region of the plug. The beam did not intercept the axis of the device (where these measurements were made) until 35 cm past the midplane of the plug. It then passed through the transition magnets into the central cell. Along this path, ions were created by charge exchange and ionization. Because these ions were injected at a shallow angle to the magnetic field (18^0), they speed along the field line until they reached the far end wall. There, their energy spectrum is measured by ELA1.

The spread in energy of these ions is a direct measure of the potential variation along the field line where they were deposited. This energy spread extends from the beam injection energy plus the potential at the bottom of the barrier up to a maximum value of the beam energy plus the central cell potential. The width of the spread in energies is the barrier depth.

The resulting measurement of the axial potential profile is shown in Fig. 5. The maximum energy in the beam spectrum corresponds to the central cell potential measured by ELA2. The lower energy part of the beam spectrum therefore corresponds to a potential depression 450 V deep in the region where we expect a thermal barrier to form.

During the time that plugging was observed, the measured barrier depth varied from approximately 100 V (which is equal to the sum of the possible measurement errors) to over 600 V. However, because this measurement required us to operate TMX-U in a single-ended configuration so that we could confirm the diagnostic beam measurement of ϕ_e, the number of measurements is limited.

A second instrument, the plasma potential diagnostic (PPD), is being brought into full operation in the central cell of TMX-U (Fig. 6). This diagnostic, similar to the heavy ion beam probe used successfully on the original TMX device,[10] and will allow us to measure the central cell potential while operating as a double-end tandem mirror. The PPD operates by injecting a beam of singly ionized thallium ions (atomic mass 204) at 46 keV into the central cell plasma (B ≈ 3 kG). Some of these ions interact with the plasma and become doubly ionized.

At the point where the ionization event occurs, the gyroradius of the thallium ion is reduced by a factor of 2. This separates the doubly charged ions (secondaries) from the incident beam (primaries). It also causes them to gain energy as they gyrate away from the point of ionization toward the wall of the central cell. The energy they gain is $\phi(x,y)$ where x,y are the co-ordinates of the point of secondary ionization. By placing an electrostatic, parallel-plate energy analyzer in the path of the secondary ions gyro-orbit, it is possible to measure the increase in the ion's energy above its injection energy and, thereby, deduce $\phi(x,y)$. It is then possible to map out the radial profile of the plasma potential by sweeping the beam through the plasma so that different points of beam plasma interaction will map into the energy analyzer.

In addition to the ELA and the PPD, we use a total of nine Langmuir probes and high-impedance probes at the plasma edge to measure the plasma floating potential and the fluctuations in the floating potential. We can also obtain a measure of the radial profile of the potential when we electrically float the plasma potential control (PPC) plates at the ends of the device.

Near each end wall of TMX-U there are concentric metal plates that can be electrically isolated from the end walls. These plates are separated into six radial zones. The plates, which comprise the outer 4 radial zones, are segmented into 4 azimuthal zones for a total of 18 electrically separated plates (per end). These plates are floated both to force the radial losses to be ambipolar[11] and to reduce the central cell potential and, thereby, decrease the magnitude of the radial electric field. The PPC plate data have shown that there are no large azimuthal asymmetries in the plasma potential, and comparisons with the potential measured by the ELA show that the plates typically float at minus 1/2 the potential measured by the ELA.

In addition to the diagnostics which we have discussed, we are developing two new diagnostics/diagnostic techniques for potential measurements in TMX-U: the end-loss-ion spectrometer (ELIS) and phase-space-dependent charge-exchange analysis (NFS).

The ELIS (Fig. 7) is a variation on the EIIB charge-exchange analyzer used on the Tokamak Fusion Test Reactor (TFTR).[12] The ELIS will be placed on the end wall of TMX-U in the same fashion as the ELA. End-loss ions and electrons enter the analyzer through a magnetically shielded aperture where they are separated by the analyzer's magnetic field. The ions then execute approximately 1/2 a gyro-orbit in the analyzer's magnetic field. In the process, they are separated in momentum by the magnetic field while they are separated by the charge-to-mass ratio in the analyzer's electric field (parallel to the magnetic field). Last, the energy- and mass-resolved ion current is collected on an etched array of Faraday cups.

In this way the ELIS measures the differential energy spectrum (dj/dE) of the end-loss ion current. Because the ELIS does not require large potentials

to sweep out the energy spectrum, problems with voltage breakdown are significantly reduced and a wide range of ion energies can be measured at one time with good time resolution. (The ELA is limited by voltage sweep rates.) The ELIS also automatically separates the electron current from the ion current; this eliminates errors that occur when super-thermal electrons (i.e., thermal barrier electrons) pass through the electron repeller grid and are collected with the ion current. This has been a problem in TMX-U when measuring the end-loss ion currents during low density operation or during periods of strong plugging of the ion end losses.

The second new potential measurement--phase-space-dependent charge-exchange analysis (NFS)--is based on the principle that the distribution function of certain ions exhibit cutoffs or clear discontinuities at energies that are determined by the spatial variations of the plasma potential. For example, there are central cell ions that have a high enough ratio of parallel energy to perpendicular energy to pass through the mirror between the central cell and the end cell but are electrostatically confined by the potential peak in the end cell. As these ions pass into the end cell, they fall through the thermal barrier and gain energy ϕ_b. They then climb the ion-confining potential peak until their parallel energy goes to zero, causing them to reverse direction and pass back into the central cell.

At the bottom of the thermal barrier, these ions cannot have an energy greater than

$$E = e\delta\phi_a + e\phi_i \left[(B_\phi - B_b)/(B_{IM} - B_\phi)\right] \quad , \tag{5}$$

where $\delta\phi_a$ is the potential difference between the bottom of the thermal barrier and the top of the ion-confining potential peak, and B_ϕ, B_b, and B_{IM} are

the magnetic field strengths at the potential peak, the bottom of the thermal barrier, and the central cell mirror, respectively.

By looking at a shallow angle (e.g., 18^{o}) to the magnetic field with a charge-exchange analyzer, it is possible to obtain a direct measure of $\delta\phi_a$ with this measurement. The thermal barrier depth is then calculated from

$$\phi_b = \delta\phi_a - (\phi_p - \phi_e) \quad , \tag{6}$$

where ϕ_e is measured by the PPD and ϕ_p is measured by the ELA. In addition, there may be a clear break in the charge-exchange flux at $E = e\phi_b$ because tnis is the characteristic energy of the barrier-trapped ions. We plan to develop this measurement technique on TMX-U.

II. PLASMA POTENTIAL DIAGNOSTICS FOR MFTF-B

Plasma potential measurements will also be important for the MFTF-B experiment now under contruction at LLNL and scheduled for initial operation in 1987 (Fig. 8). However, these measurements will be more challenging on MFTF-B than TMX-U because of:

- The size of the device. (MFTF-B is 10.6 m in diameter and 58 m long.)
- The necessity of remote-operation diagnostics. (The vault will not be accessible during machine operation.)
- The magnitude of the potentials (up to 80 kV) and magnetic fields. (The minimum field in the confinement region is 10 kG.)
- The complexity of the device. (MFTF-B adds a "transition" region that TMX-U does not have at this time.)

The basic potential diagnostics planned for MFTF-B are end-loss-ion spectroscopy (ELIS), phase-space-dependent charge-exchange analysis (NSF), plasma potential control (PPC) plates for measuring the potential in the interior of the plasma, and Langmuir probes for measuring the floating potential at the plasma edge. The basic diagnostic set for MFTF-B calls for an array of seven ELIS instruments on one end wall and two on the other to determine the radial profile of the plug potential during normal operation as well as the radial profile of the central cell potential during single-end plug operation. In addition, the ELIS diagnostics that collect ions from the high energy pump beam/plasma interaction will measure the radial profile of $\delta\phi_a$.

A total of 6 NFS detectors are to be used on MFTF-B to measure the ion-confining potential and $\delta\phi_a$ on each end of the device. The seventh will measure the central cell ion temperature. Radial profiles of these potentials will be determined by radially sweeping the NFS diagnostics on a shot-to-shot basis. New plasma potential diagnostics that would augment the measurements of these diagnostics are highly desirable.

III. SUMMARY

We have examined the theoretical basis for thermal barrier formation in a tandem mirror and reviewed the diagnostics on TMX-U which have shown that a thermal barrier was formed in the device. We have also looked briefly at the basic diagnostic set for MFTF-B and discussed how plasma potential measurements would be more difficult on MFTF-B than on TMX-U. We note, however, that these measurements will continue to be important to the understanding of plasma confinement in tandem mirrors.

IV. ACKNOWLEDGMENTS

The author gratefully acknowledges the contributions of the tandem mirror physics and engineering teams who made the plasma potential measurements possible. This was a team accomplishment. The author would particularly like to acknowledge those people who took primary responsibility for the potential diagnostics: A. W. Molvik, design of the ELA; J. H. Foote, development of the ELIS; R. S. Hornady, PPD; E. B. Hooper, PPC plates; W. Hsu, Langmuir probes; T. A. Casper, high-impedance probes; and G. W. Leppelmeier, J. E. Osher, and M. Carter, NFS.

This work was performed under the auspices of the U.S. Department of Energy by the Lawrence Livermore National Laboratory under contract number W-7405-ENG-48.

REFERENCES

[1] V. P. Pastukov, Nucl. Fusion 14, 3 (1974).

[2] D. L. Correll, S. L. Allen, T. A. Casper, J. F. Clauser, P. Coakley, F. H. Coensgen, W. Condit, W. F. Cummins, J. C. Davis, R. P. Drake, J. H. Foote, A. H. Futch, R. K. Goodman, D. P. Grubb, G. A. Hallock, E. B. Hooper, R. S. Hornady, A. L. Hunt, C. V. Karmendy, A. W. Molvik, W. E. Nexsen, W. L. Pickles, P. Poulsen, T. C. Simonen, B. W. Stallard, and O. T. Strand, Nucl. Fusion 22, 223 (1982).

[3] K. Yatsu, S. Miyoshi, H. Tamai, K. Shida, K. Ishii, and A. Itakura, Phys. Rev. Lett. 43, 627 (1979).

[4]R. Breun, S. N. Golovato, L. Yujiri, B. McVey, A. Molvik, D. Smatlak, R. S. Post, D. K. Smith, and N. Hershkowitz, Phys. Rev. Lett. 47, 1833 (1981).

[5]D. E. Baldwin and B. G. Logan, Phys. Rev. Lett. 43, 1318 (1979)

[6]D. P. Grubb, S. L. Allen, T. A. Casper, J. F. Clauser, F. H. Coensgen, D. L. Correll, W. F. Cummins, C. C. Damm, J. H. Foote, R. K. Goodman, D. N. Hill, E. B. Hooper, Jr., R. S. Hornady, A. L. Hunt, R. G. Kerr, G. W. Leppelmeier, J. Marilleau, J. M. Moller, A. W. Molvik, W. E. Nexsen, W. L. Pickles, G. D. Porter, P. Poulsen, E. H. Silver, T. C. Simonen, B. W. Stallard, W. C. Turner, W. L. Hsu, T. L. Yu, J. D. Barter, T. Christensen, G. Dimonte, T. W. Romesser, R. F. Ellis, R. A. James, C. J. Lasnier, L. V. Berzins, M. R. Carter, C. A. Clower, B. H. Failor, S. Falabella, M. Flammer, and T. Nash, Phys. Rev. Lett. 53, 785 (1984).

[7]R. H. Cohen, I. B. Bernstein, J. J. Dorning, and G. Rowlands, Nuc. Fusion 20, 1421 (1980).

[8]R. H. Cohen, Phys. Fluids 26, 1997 (1983); Y. Matsuda and T. D. Rognlien, Phys. Fluids 26, 1778 (1983).

[9]A. W. Molvik, Rev. Sci. Instrum. 52, 704 (1981).

[10]G. A. Hallock, "Radial Space Potential Measurements in the Central Cell of the Tandem Mirror Experiment with a Heavy Ion Beam Probe," Lawrence Livermore National Laboratory, Livermore, CA, UCID-19759 (1983).

[11]E. B. Hooper, Jr., D. E. Baldwin, T. K. Fowler, R. J. Kane, and W. C. Turner; to be published in Phys. Fluids.

[12]Sid Medley, "Use of the TFTR Prototype Charge Exchange Neutral Analyzer for Fast He_3^{++} Diagnostics During ICRF Heating on PLT," Princeton Plasma Physics Lab., Princeton, NJ, PPPL-1770 (1981).

4508v/MM

FIGURE CAPTIONS

Fig. 1. Thermal barrier in a TMX-U end cell (theoretical model) showing axial profiles of (a) the magnetic field and plasma potential, (b) the three species of electrons, and (c) the three species of ions.

Fig. 2. The location of TMX-U plasma potential diagnostics referenced to the walls of the vacuum vessel and the magnets.

Fig. 3. Gridded, electrostatic energy analyzer (ELA).

Fig. 4. Time history of (a) the current received by the ELA collector and the voltage on the ion repeller (see Fig. 3) and (b) current vs voltage for the voltage sweep indicated by the arrows in this figure.

Fig. 5. Single-end tandem configuration of TMX-U (a) used for thermal barrier potential measurements. In (b) the measured potentials (X's) are placed on the theoretically predicted axial variation of the plasma potential (solid line).

Fig. 6. Plasma potential diagnostic (PPD) in the TMX-U central cell.

Fig. 7. The EIIB end-loss ion spectrometer.

Fig. 8. Axial variation of the magnetic field and plasma potential (theoretical model) in MFTF-B.

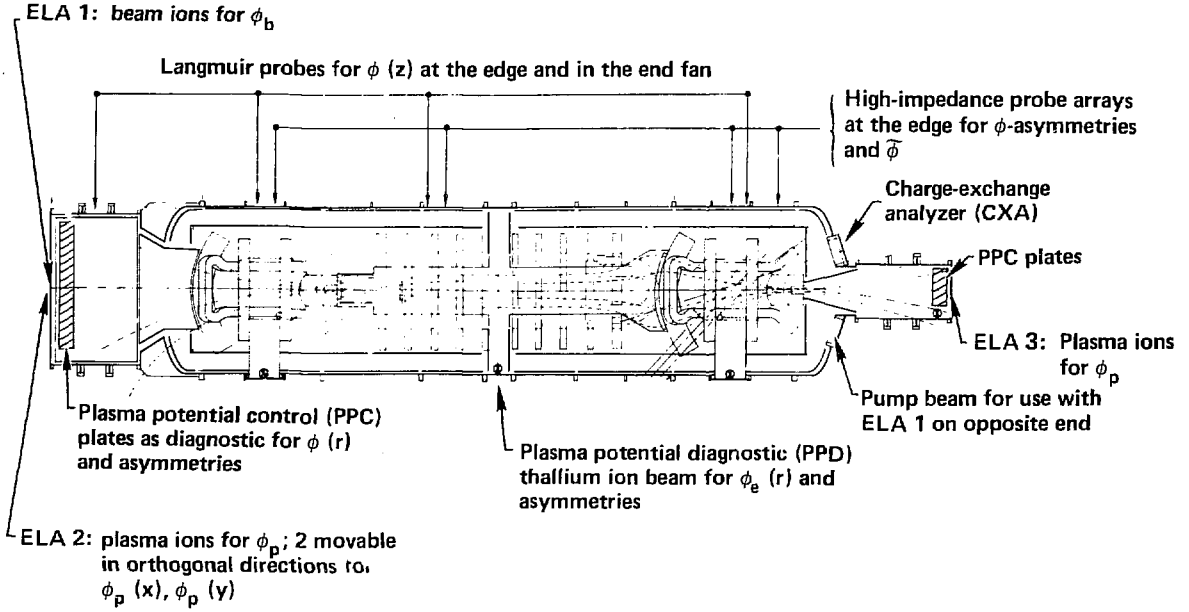

D. P. Grubb - Figure 2

D. P. Grubb - Figure 3

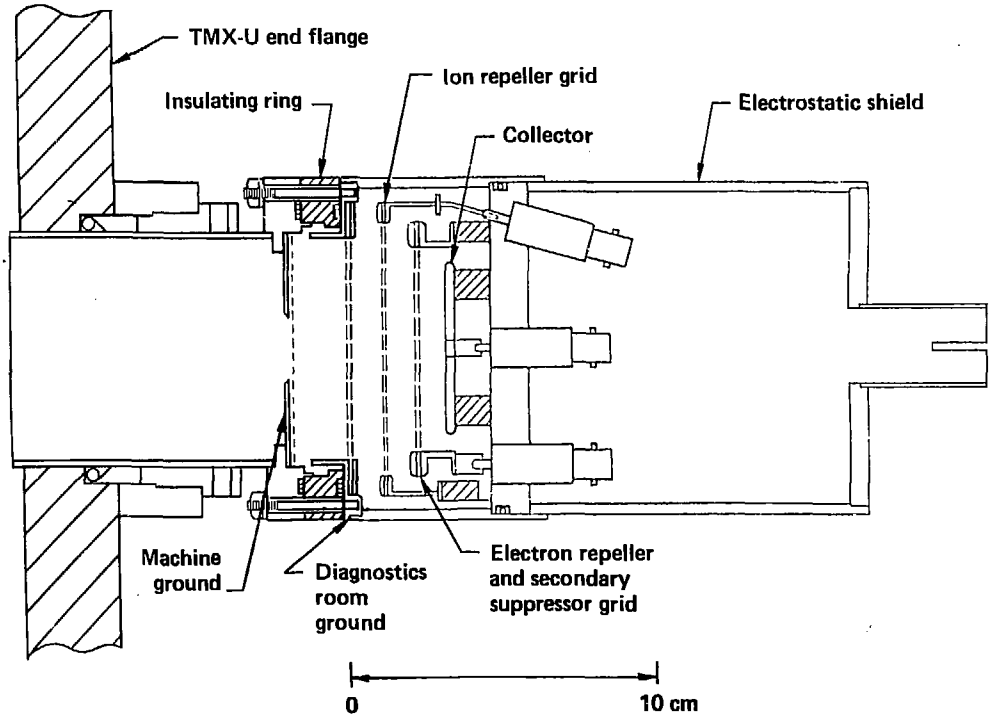

D. P. Grubb - Figure 4

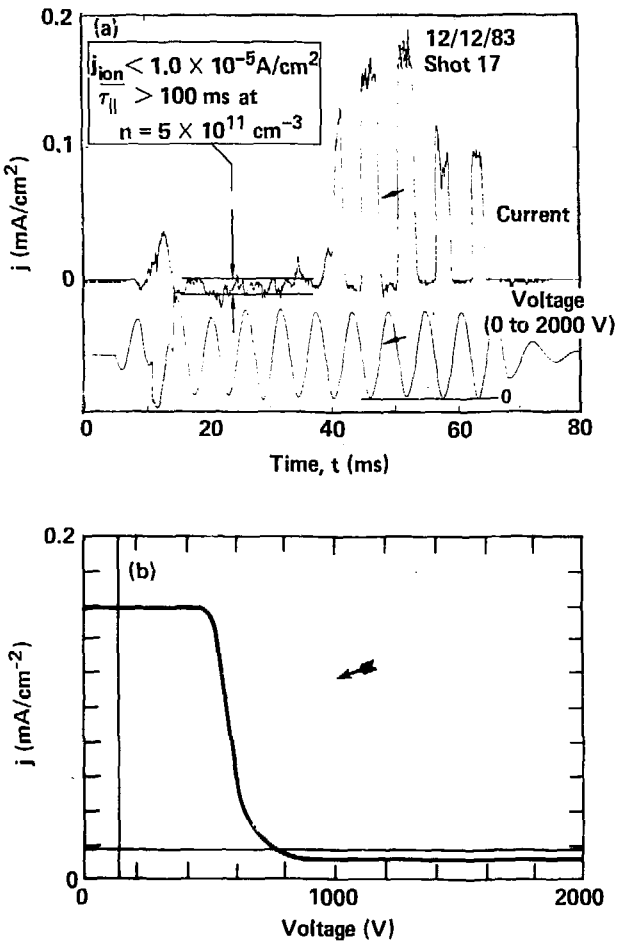

D. P. Grubb - Figure 5

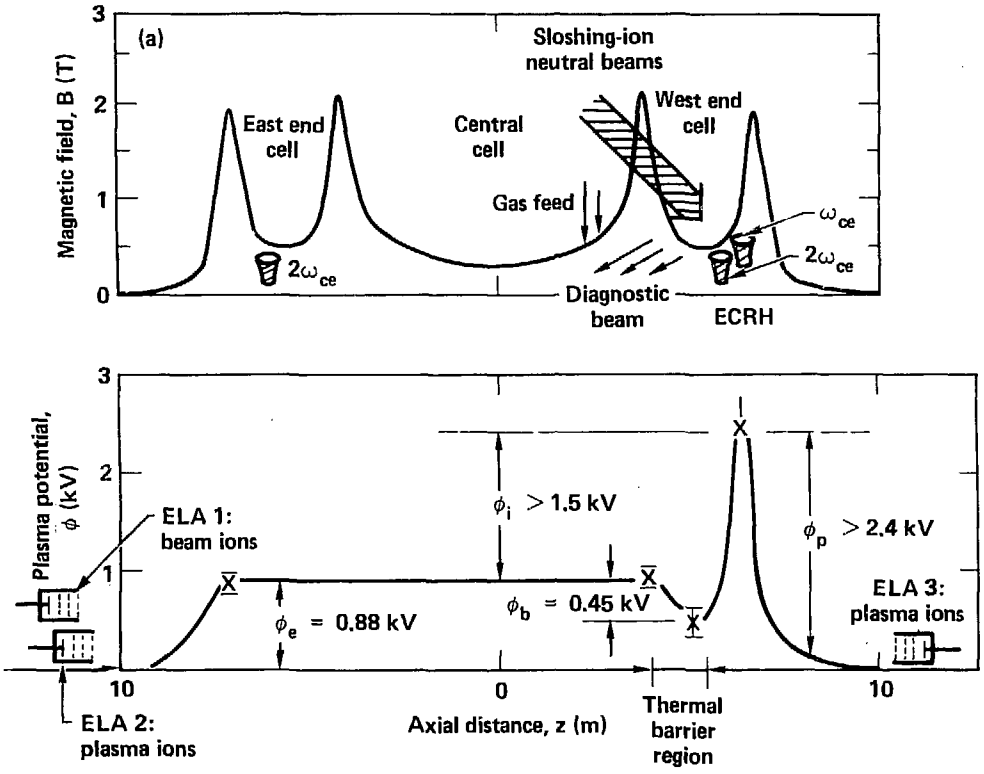

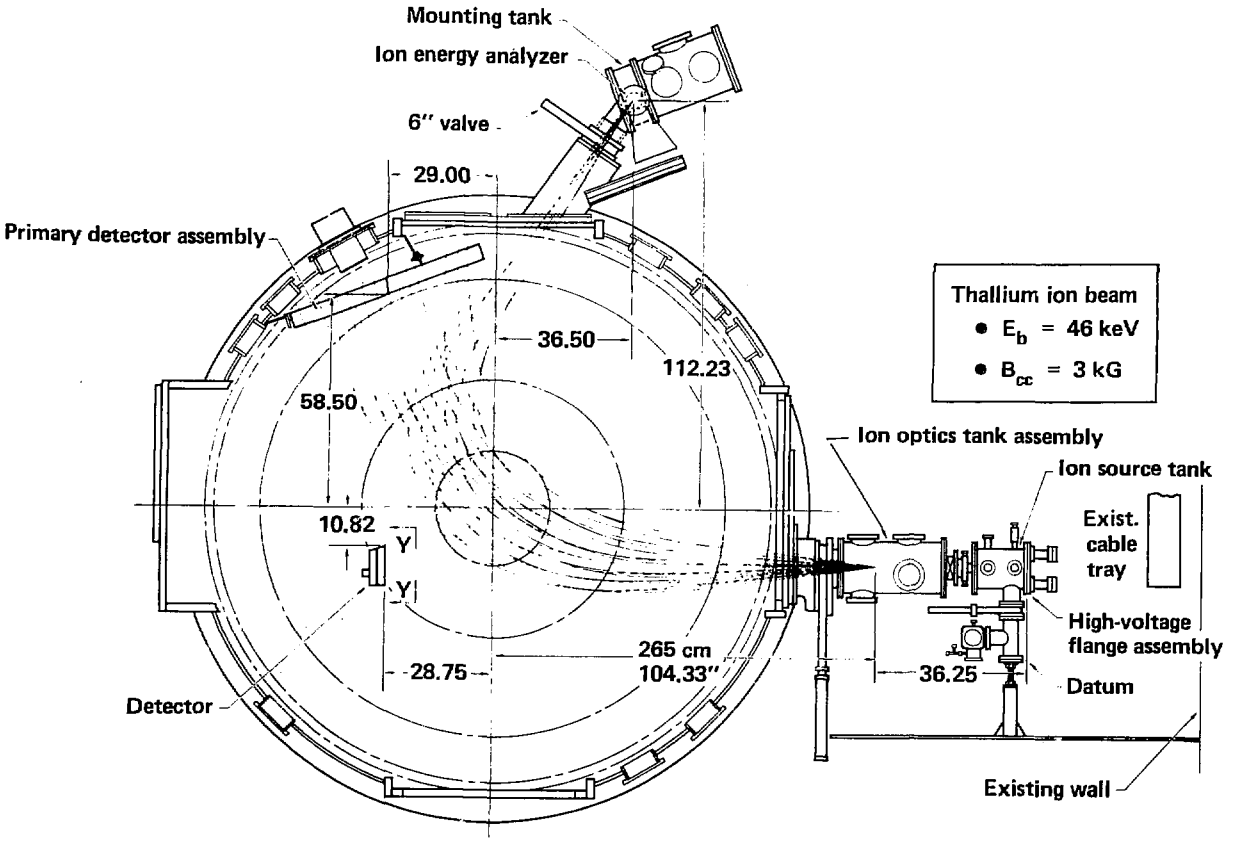

D. P. Grubb - Figure 6

D. P. Grubb - Figure 7

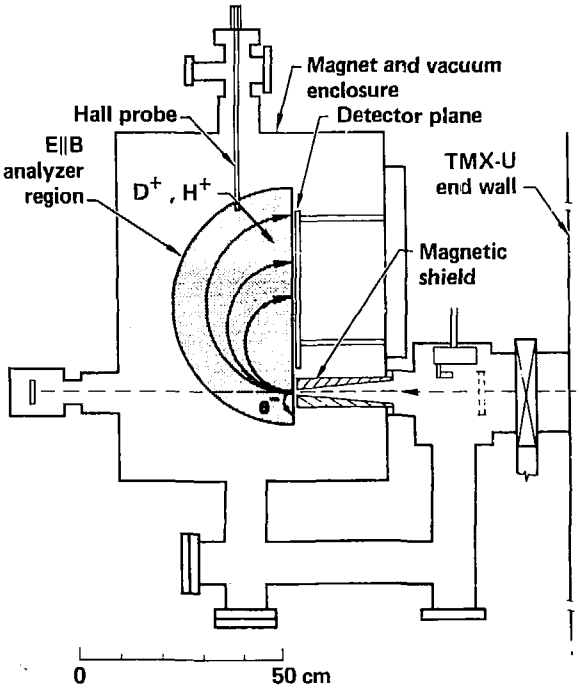

D. P. Grubb - Figure 8